Ionics (2018) 24:3705–3715
https://doi.org/10.1007/s11581-018-2553-z

ORIGINAL PAPER

The multiple effects of Al-doping on the structure and electrochemical performance of $LiNi_{0.5}Mn_{0.5}O_2$ as cathode material at high voltage

Guofeng Jia[1,2,3] · Suqin Liu[1,4] · Guowei Yang[2,3,5] · Faqiang Li[2,3] · Kang Wu[2,3,5] · Zhen He[1,4] · Xuehui Shangguan[2,3,5]

Received: 1 March 2018 / Revised: 30 March 2018 / Accepted: 3 April 2018 / Published online: 16 May 2018

Abstract

The application of $LiNi_{0.5}Mn_{0.5}O_2$ as a high-voltage cathode material for lithium-ion batteries is limited by its poor cycle performance. Therefore, we attempt to improve the cyclability of this material at high voltage by using a doping method and propose a detailed mechanism for the effect of the doping amount on the structure and electrochemical performance. In this work, $LiNi_{0.5-z}Al_zMn_{0.5}O_2$ ($z = 0.00$, 0.03, 0.05, 0.08) electrodes were prepared via a simple co-precipitation followed by a solid-state method. X-ray diffraction and Rietveld refinement revealed that a suitable amount of Al doping into $LiNi_{0.5}Mn_{0.5}O_2$ can stabilize the structure and lower the Li/Ni cation mixing, but an excessive doping would lead to Al-ion doping in the lithium layer, which can block lithium diffusion and affect the rate property. Specifically, $LiNi_{0.47}Al_{0.03}Mn_{0.5}O_2$ shows a much higher capacity retention compared to $LiNi_{0.5}Mn_{0.5}O_2$ both at 25 °C (78.5 vs. 68.8% at 0.2 C) and 60 °C (70.8 vs. 69.0% at 0.2 C). Moreover, Al-doping can retard the voltage drop during the discharge-charge state, with the discharge voltage for $LiNi_{0.5-z}Al_zMn_{0.5}O_2$ ($z = 0.00$, 0.03, 0.05, 0.08) decreasing slowly with increasing Al content.

Keywords Lithium-ion battery · $LiNi_{0.5}Mn_{0.5}O_2$ cathode material · Al-doping · High-voltage · Structural changes

Introduction

Rechargeable lithium-ion batteries (LIBs) have received significant attention in past 20 years for use in energy storage devices in the field of portable electronics because of their high power and energy density [1–3]. $LiCoO_2$ as the main commercial cathode material shows several inherent disadvantages such as low charge-discharge capacity, high cost and toxicity [4–6]. Consequently, $LiCoO_2$ cannot be used in many higher powered machines such as electric vehicles and hybrid electric vehicles.

To solve these problems, many alternative cathode materials have been investigated over the years especially manganese oxide-based layered materials [7–9]. The structure of manganese oxide-based layered materials is similar to $LiCoO_2$ [10, 11]. $LiNi_{0.5}Mn_{0.5}O_2$, in which nickel (Ni) is divalent and manganese (Mn) is tetravalent, is a potential candidate for the replacement of $LiCoO_2$ due to inherent advantages such as low-cost, low-toxicity, high-energy density and increased safety [12–14]. In addition, $LiNi_{0.5}Mn_{0.5}O_2$ shows only small volume changes

Electronic supplementary material The online version of this article (https://doi.org/10.1007/s11581-018-2553-z) contains supplementary material, which is available to authorized users.

✉ Suqin Liu
sqliu2003@126.com

[1] College of Chemistry and Chemical Engineering, Hunan Provincial Key Laboratory of Chemical Power Sources, Central South University, Changsha, Hunan 410083, People's Republic of China

[2] Key Laboratory of Comprehensive and Highly Efficient Utilization of Salt Lake Resources, Qinghai Institute of Salt Lakes, Chinese Academy of Sciences, Xining, Qinghai 810008, People's Republic of China

[3] Key Laboratory of Salt Lake Resources Chemistry of Qinghai Province, Xining 810008, People's Republic of China

[4] Hunan Provincial Key Laboratory of Efficient and Clean Utilization of Manganese Resources, Changsha, Hunan 410083, People's Republic of China

[5] University of Chinese Academy of Sciences, Beijing 100049, People's Republic of China

during the charge-discharge process [15]. However, $LiNi_{0.5}Mn_{0.5}O_2$ as cathode material still has some problems. Firstly, Ni^{2+} becomes Ni^{4+} in the charged state, which is too unstable to react with the electrolyte, leading to a severe decrease in capacity [16, 17]. Secondly, $LiNi_{0.5}Mn_{0.5}O_2$ without Co shows low conductivity, which results in a relatively poor rate capability [18–20]. Most importantly, Li^+ (radius = 0.076 nm) and Ni^{2+} (radius = 0.069 nm) both have similar radii, leading to Li/Ni cation mixing, which results in a slow charge-discharge speed and lower capacity [21–23].

With respect to the disadvantages of $LiNi_{0.5}Mn_{0.5}O_2$, nanostructuring, carbon coating, and elemental doping are all useful for improving the material weaknesses to a certain extent. However, nanostructures can also show weaknesses, including side reactions and volume swelling [24, 25]. Moreover, carbon coating may reduce the top density, which can thus reduce the energy density. It is believed that metal doping can be used to stabilize the layered framework. Attempts to improve the cyclability of layered materials by doping have been reported in several studies. Elemental doping using Mg^{2+} [26], Al^{3+} [27], Cr^{3+} [28], Ti^{3+} [29], or other ions [30–32] is much more straightforward and useful for improving the properties of lithium-ion batteries, which can lower the degree of Li/Ni cation mixing and alleviate voltage degradation. Xiao et al. proposed Mg-ion substitution for the Ni-ion in $LiNi_{0.5}Mn_{0.5}O_2$, which can maintain a stable structure due to the higher bond dissociation energy for Mg-O (394 kJ mol^{-1}) compared to Ni-O (391.6 kJ mol^{-1}), improving the cycle stability [26]. Chen et al. showed that Ca-doping into $LiNi_{0.8}Co_{0.1}Mn_{0.1}O_2$ can improve the electrochemical performance by decreasing the degree of Li/Ni cation maxing [30].

Ceder et al. demonstrated that Al-ion substitution for the Co-ion in $LiCoO_2$ can be used to increase the potential [17]. Myung et al. reported that $LiNi_{0.475}Al_{0.05}Mn_{0.475}O_2$ prepared by doping Al-ion into $LiNi_{0.5}Mn_{0.5}O_2$ can reduce Li/Ni cation mixing, enhancing the discharge capacity and cycle stability [33]. In this work, Al-ion doping into $LiNi_{0.5}Mn_{0.5}O_2$ is achieved by preparing $LiNi_{0.5-z}Al_zMn_{0.5}O_2$ (z = 0.00, 0.03, 0.05, 0.08) using a simple co-precipitation and the solid-state method to realize a longer cycle life with minimum capacity loss and smaller voltage decay in the high-voltage range of 3.0~4.8 V. Most importantly, the structural changes produced by the Al-ion doping in $LiNi_{0.5}Mn_{0.5}O_2$ were investigated through X-ray diffraction and Rietveld refinement and analyzed in detail before and after cycling. Cyclic performance and voltage retention properties were studied through a charge-discharge test. In addition, this study proposed a detailed mechanism for the effect of the doping amount on the structure and electrochemical performance.

Experimental section

Materials preparation

Synthesis of $Ni_{0.5-z}Al_zMn_{0.5}CO_3$

Manganese sulfate [$MnSO_4 \cdot H_2O$], nickel sulfate [$NiSO_4 \cdot 6H_2O$], crystalline aluminum chloride [$AlCl_3 \cdot 6H_2O$], and sodium carbonate [Na_2CO_3] were used as starting materials for synthesizing $Ni_{0.5-z}Al_zMn_{0.5}CO_3$ (z = 0.00, 0.03, 0.05, 0.08) by a combination of co-precipitation and solid-state reaction. Firstly, stoichiometric amounts of the starting materials were weighed out. Next, $MnSO_4 \cdot H_2O$, $NiSO_4 \cdot 6H_2O$, and $AlCl_3 \cdot 6H_2O$ were dissolved in 30.0 ml of deionized water, Na_2CO_3 was dissolved separately in 20.0 ml of deionized water, and the precursor solution was mixed with Na_2CO_3 in a molar ratio of 1:2. Then, the Na_2CO_3 solution was very slowly added into the mixture under violent stirring. After stirring for 12 h, the mixture was filtered, washed with deionized water three times, and dried for 12 h at 80 °C. Finally, $Ni_{0.5-z}Al_zMn_{0.5}CO_3$ (z = 0.00, 0.03, 0.05, 0.08) was obtained.

Synthesis of $LiNi_{0.5-z}Al_zMn_{0.5}O_2$

$Ni_{0.5-z}Al_zMn_{0.5}CO_3$ and lithium hydroxide [$LiOH \cdot H_2O$] were mixed together and milled more completely with a molar ratio of 1:1.05. The resulting mixture was then calcinated at 500 °C for 5 h in air with a temperature ramp rate of 5 °C min^{-1} and then at 850 °C for 12 h in air with the same heating rate to obtain $LiNi_{0.5-z}Al_zMn_{0.5}O_2$ (z = 0.00, 0.03, 0.05, 0.08).

Material characterization

The structures of the as-synthesized sample were measured by X-ray diffraction (Persee XD2) using Cu-Kα radiation (α = 1.5418) at 40 kV and 40 mA at room temperature. The diffraction data were obtained in the range of 10~80°.

Electrochemical measurement

The cathode materials were prepared by a slurry coating procedure. The slurry was prepared by mixing together 80 wt% cathode material, 10 wt% carbon black, and 10 wt% polyvinylidene fluoride (PVDF). The resulting slurry was dissolved in N-methyl pyrrolidinone (NMP) and then evenly spread onto aluminum (Al) foil. Next, the coated sample was dried at a temperature of 80 °C for approximately 60 min. Finally, the sample was dried under vacuum at 120 °C for 12 h. Disc electrodes with a diameter of 12 mm were used to assemble 2025 coin-type cells. The loading density of the composite electrode was around 1.8 mg cm^{-2}.

Half cells were assembled using the as-prepared $LiNi_{0.5-z}Al_zMn_{0.5}O_2$ (z = 0.00, 0.03, 0.05, 0.08) as cathode, Celgard

2400 polypropylene film as separator, and lithium foil as anode. Charge-discharge performance was investigated for $Li|LiNi_{0.5-z}Al_zMn_{0.5}O_2$ ($z = 0.00$, 0.03, 0.05, 0.08) cells using a LAND CT2001A Battery Test System (Wuhan, China) at room temperature or 60 °C between 3 and 4.8 V (vs. Li/Li^+) using an automatic galvanostat. Long-term cycling tests were carried out at rates of 0.2 C for 150 cycles. In addition, electrochemical impedance spectroscopy (EIS) was carried out using a PMC1000 electrochemical workstation (Princeton, USA) in the frequency range between 0.1 and 10^5 Hz using a voltage with amplitude of 5 mV.

Results and discussion

Structural character

Figure 1a shows the XRD patterns obtained for $LiNi_{0.5-z}Al_zMn_{0.5}O_2$ powders with $z = 0.00$, 0.03, 0.05, and 0.08, which are all synthesized by a combination of co-precipitation and solid-state reaction. The data show clear peaks labeled (006)/(102) and (003)/(104), which are the main characteristics for a layered hexagonal type structure [34]. As shown in Fig. 1a, all of these peaks are narrow and sharp, which indicates that the materials have high crystallinity. Moreover, all the diffraction peaks of the material show a powder phase with a hexagonal unit cell (α-$NaFeO_2$ type structure) with a space group R-3 m. Specifically, these data show that the material has good cation ordering because the intensity of (003) is higher than (104). In addition, the intensity ratio of $I_{(003)}/I_{(104)}$ directly suggests cation mixing within the structure, which related to cathode electrochemical performance [35]. On this point, our sample suggests a little Ni^{2+} occupies the place of Li^+ in the crystals. To study structural changes after doping in detail, the partially enlarged graphs for the (003), (101), and (104) diffraction peaks are also shown (Fig. 1b). According to previous studies, a diffraction peak corresponding to an angle bigger than 2θ in the XRD pattern indicates a smaller interplanar spacing, with the reverse also true [36]. A spot of doping ($0.00 < z \le 0.03$) leads to no clear shift in the (003) diffraction peaks relative to the pristine material. For increasing z ($0.05 \le z \le 0.08$), the spacing of (003) transforms to a slightly smaller 2θ angle. Thus, a small quantity of Al-doping cannot be used to enlarge the spacing of the lithium layers; however, as the quantity of doping increases, the Al-ion can increase the spacing of the (003) slab. However, the both (101) and (104) peaks shift to a bigger 2θ angle with doping. The detail effect of Al-ion doped in $LiNi_{0.5-z}Al_zMn_{0.5}O_2$ was systematically investigated in the following section. SEM measurements with pristine and $LiNi_{0.47}Al_{0.03}Mn_{0.5}O_2$ and elemental mapping can be seen in Fig. S1(a–k).It can be seen that doped sample have similar morphologies, which suggests that Al^{3+} permeated into the material and formed a solid solution, and the corresponding elements are distributed equally.

To verify the expected Al^{3+} substitution for Ni^{2+}, we analyze the XRD patterns obtained for the synthesized materials by Rietveld refinement, as shown in Fig. 2. The results are summarized in Table 1. The data show the crystal cell parameters for the synthesized $LiNi_{0.5-z}Al_zMn_{0.5}O_2$ ($z = 0.00$, 0.03, 0.05, 0.08). When z increases, the value of the cell parameters a, c, and V will decrease. This is because the radius of Al^{3+} (radius = 0.057 nm) is smaller than Ni^{2+} (radius = 0.069 nm). Therefore, the cell volume will decrease with increasing number of Al^{3+} ions. This indicates substitution of Al^{3+} for a fraction of Ni^{2+} ions. Moreover, previous researches indicated that a $I_{(003)}/I_{(104)}$ ratio of 1.2 or above indicates good cation ordering [35]. In our sample, both the c/a and $I_{(003)}/I_{(104)}$ ratios increased with increasing doping content, which indicates a reduction in Li/Ni mixing. As shown in Table 1, $(I_{(006)} + I_{(102)})/I_{(101)}$ decreased with increasing doping content, which illustrates higher ordering of the hexagonal structure induced by doping [37]. These small but significant differences among the four materials may lead to different electrochemical performances. As shown in Fig. 3, compared to the pristine sample, the transitional metal

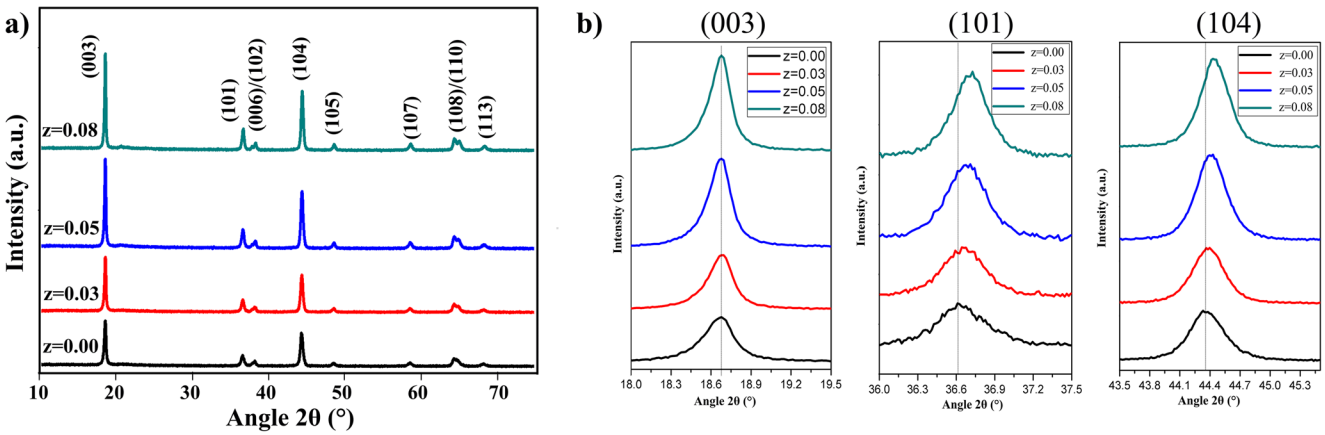

Fig. 1 **a** X-ray diffraction patterns for $LiNi_{0.5-z}Al_zMn_{0.5}O_2$ ($z = 0.00$, 0.03, 0.05, 0.08). **b** Partially enlarged detail for the (003), (101), and (104) diffraction peaks

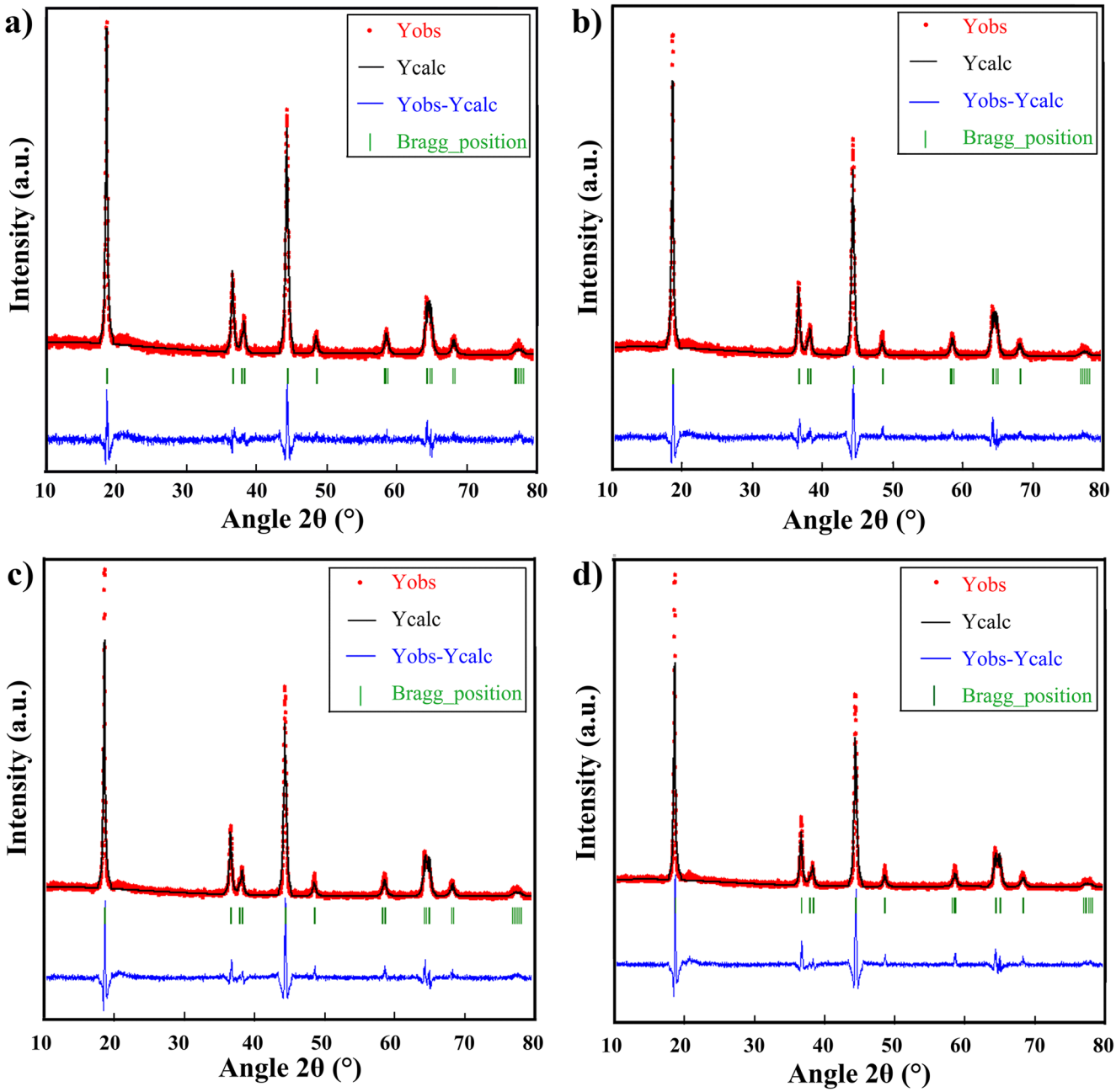

Fig. 2 Rietveld refinement of the X-ray diffraction patterns for the $LiNi_{0.5-z}Al_zMn_{0.5}O_2$ ($z = 0.00, 0.03, 0.05, 0.08$) samples. **a** $z = 0.00$, **b** $z = 0.03$, **c** $z = 0.05$, **d** $z = 0.08$

Table 1 The Rietveld refinement results obtained for $LiNi_{0.5-z}Al_zMn_{0.5}O_2$ ($z = 0, 0.03, 0.05, 0.08$)

	$z = 0.00$	$z = 0.03$	$z = 0.05$	$z = 0.08$
a (Å)	2.8803	2.8760	2.8737	2.8723
c(Å)	14.2605	14.2542	14.2501	14.2491
V (Å^3)	102.457	102.107	101.916	101.804
c/a	4.9510	4.9562	4.9587	4.9631
$I_{(003)}/I_{(104)}$	1.3007	1.4104	1.4799	1.5380
$(I_{(006)} + I_{(102)})/I_{(101)}$	1.2218	1.1553	1.0908	0.9745
Rwp (%)	12.6	7.24	7.78	8.96

layer of the doped sample is decreased, which indicates that the Al-ion is doped into the crystal lattice.

Electrochemical performance

Figure 4 shows the charge-discharge capacity of the $LiNi_{0.5-z}Al_zMn_{0.5}O_2$ positive electrode for $z = 0$, 0.03, 0.05, and 0.08 in the voltage range of 3.0~4.8 V at a constant density of 0.2 C (1 C = 160 mAh g^{-1}) for the first cycle. The data show an efficiency of 54.26, 52.39, 51.58, and 47.41%, respectively, which becomes poorer with increasing doping content. One reason for

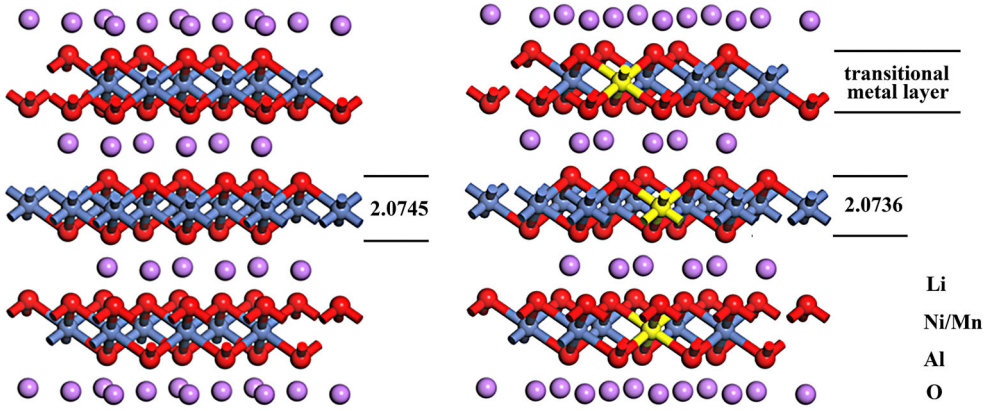

Fig. 3 Crystal structure of **a** $LiNi_{0.5}Mn_{0.5}O_2$ and **b** $LiNi_{0.47}Al_{0.03}Mn_{0.5}O_2$

this decreased efficiency is the lack of electrochemical activity for Al^{3+}. Therefore, adding or removing Al^{3+} cannot be used to improve the property of the material. Another possible reason for the poor efficiency is that a portion of the Al-ion dopants is incorporated into the lithium layer, which can block lithium diffusion. Wang et al. [36] indicated that some dopant ions preferentially dope into the transitional metal layer, which, in itself, cannot block lithium diffusion. However, some dopant elements do appear in the lithium layer, seriously hindering lithium transportation. From Fig. 1b, (101) and (104) diffraction peaks shift to a larger 2θ angle with increasing doping concentration; this phenomenon reveals that a fraction of the Al-ion dopants enter into the lithium layer, hindering the migration of lithium ions; therefore, the initial coulombic efficiency is inversely proportional to the doping amount.

The electrochemical performance of $Li|LiNi_{0.5-z}Al_zMn_{0.5}O_2$ ($z = 0.00$, 0.03, 0.05, 0.08) cells at different temperatures was measured by galvanostatic charge-discharge, with the results shown in Fig. 5. Figure 5a shows the discharge capacity of a $LiNi_{0.5-z}Al_zMn_{0.5}O_2$ positive electrode for $z = 0$, 0.03, 0.05, 0.08 in the voltage range of 3.0~4.8 V at a constant density

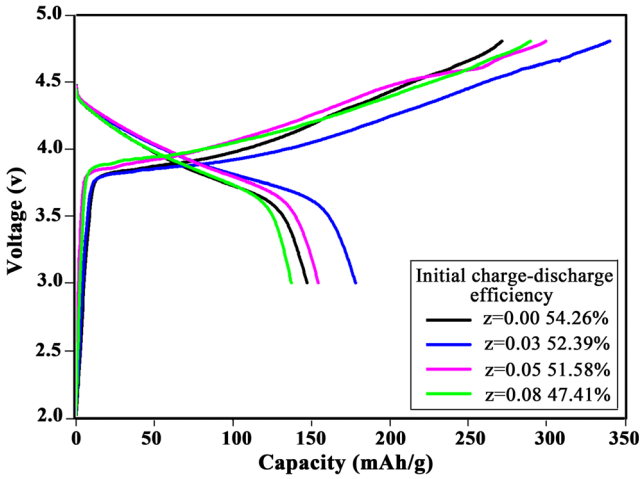

Fig. 4 Initial charge-discharge curves for $LiNi_{0.5-z}Al_zMn_{0.5}O_2$ ($z = 0.00$, 0.03, 0.05, 0.08) measured between 3.0 and 4.8 V (vs. Li^+/Li) at a current density of 0.2 C. 1 C = 160 mA g^{-1}

0.2 C measured over 150 cycles at room temperature. The data show that the $LiNi_{0.5}Mn_{0.5}O_2$ delivers a first-cycle discharge capacity of 147.5 mAh g^{-1}. After approximately 30 cycles, the discharge capacity increases to a maximum value of 167.2 mAh g^{-1}. However, the discharge capacity decreases to 101.5 mAh g^{-1} after 150 cycles, with approximately 68.81% of the original capacity maintained, which indicates a poor circulation performance. The $LiNi_{0.47}Al_{0.03}Mn_{0.5}O_2$ has a discharge capacity of 178.4 mAh g^{-1} for the first cycle, which was the best discharge capacity measured in all the cells, with a maximum capacity of 185.4 mAh g^{-1} reached after 32 cycles. Furthermore, this electrode also shows the largest capacity of 140.1 mAh g^{-1} after 150 cycles, with a capacity retention of 78.53%. The $LiNi_{0.45}Al_{0.05}Mn_{0.5}O_2$ shows a discharge capacity of 154.6 mAh g^{-1} for the first cycle. This value decreases to 127.5 mAh g^{-1} after 150 cycles, with a capacity retention of 82.47% after 150 cycles. The $LiNi_{0.42}Al_{0.08}Mn_{0.5}O_2$ shows the worst discharge capacity of 137.4 mAh g^{-1}, with only 110.0 mAh g^{-1} remaining after 150 cycles, and a capacity retention of 80.06%. The results show that the doped materials have better retention capacity compared to the pristine electrode. This is because the bond dissociation energy of Al-O (512.0 KJ mol^{-1}) is larger than that of Ni-O (382.0 KJ mol^{-1}), and Al-doping can improve the structural stability. Since $LiNi_{0.47}Al_{0.03}Mn_{0.5}O_2$ shows the best cycling performance, we chose this material to test at a higher temperature (60 °C). Figure 5b shows the cycling performance of pristine and $LiNi_{0.47}Al_{0.03}Mn_{0.5}O_2$ samples at 60 °C. The initial discharge capacities were 202.5 mAh g^{-1} and 215.3 mAh g^{-1}, respectively. After 60 charge/discharge cycles at 0.2 C, the $LiNi_{0.47}Al_{0.03}Mn_{0.5}O_2$ material delivers a specific capacity as high as 152.5 mAh g^{-1}, with a capacity retention of 70.83%. For comparison, the pristine material shows a discharge capacity of 139.8 mAh g^{-1}, with a loss of 30.96% after 60 cycles.

Figure 5c and d show the rate capability of $LiNi_{0.5}Mn_{0.5}O_2$ and $LiNi_{0.47}Al_{0.03}Mn_{0.5}O_2$ electrodes between 3.0 and 4.8 V at a current rate of 0.2 C, 0.5 C, 1 C, and 2 C at room temperature and 60 °C. As shown in Fig. 5c, at room temperature, the $LiNi_{0.47}Al_{0.03}Mn_{0.5}O_2$ electrode delivers discharge capacities

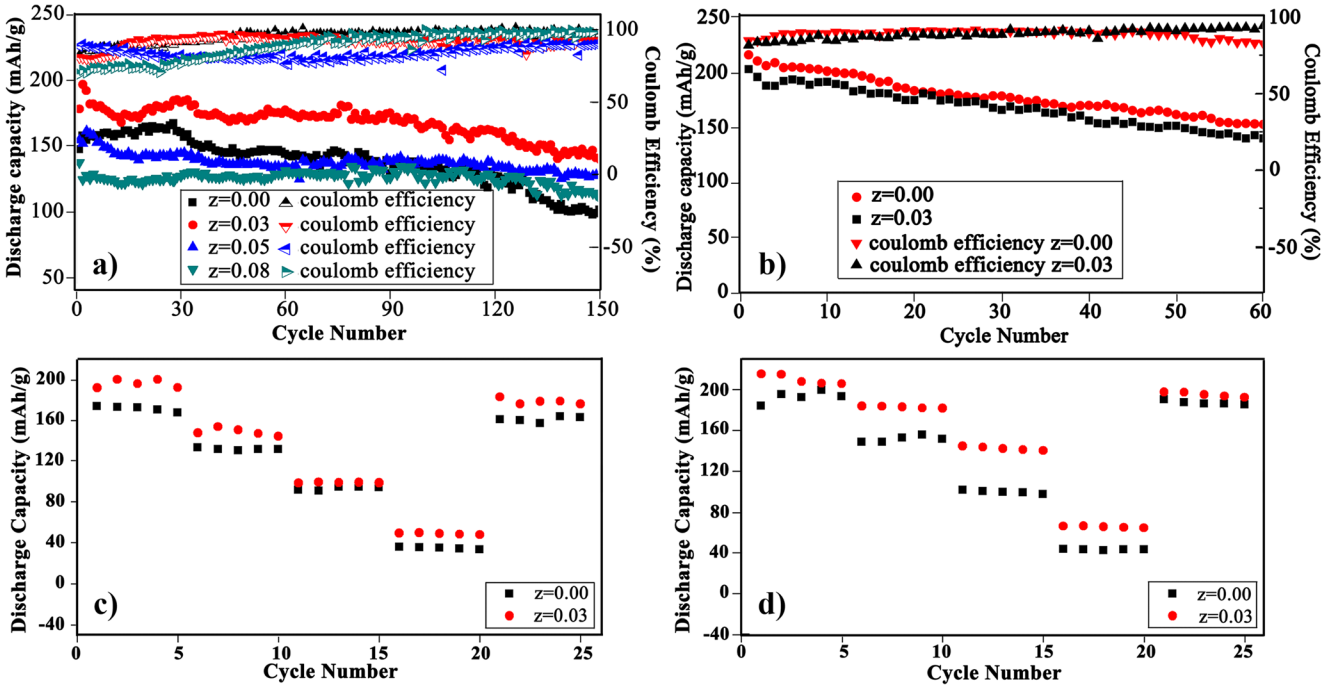

Fig. 5 Discharge capacity curve for $LiNi_{0.5-z}Al_zMn_{0.5}O_2$ ($z = 0.00, 0.03, 0.05, 0.08$) in the voltage range of 3.0~4.8 V at a constant current of 0.2 C at **a** room temperature and **b** 60 °C. Discharge capacity at current densities of 0.2 C, 0.5 C, 1 C, 2 C, 0.2 C at **c** room temperature, and **d** 60 °C

of 199.9, 153.5, 99.1, and 49.3 mAh g^{-1} at 0.2 C, 0.5 C, 1 C, and 2 C. The charge capacities of $LiNi_{0.5}Mn_{0.5}O_2$ are 173.5, 132.9, 91.6, and 35.7 mAh g^{-1} at 0.2 C, 0.5 C, 1 C, and 2 C. Therefore, the $LiNi_{0.47}Al_{0.03}Mn_{0.5}O_2$ electrode demonstrates a higher capacity at varying current rates compared to the pristine electrode. This reason for this high capacity is also due to the doping (which can keep the structure stable and lower Li/Ni cation mixing) and the higher bond dissociation energy for Al-O. Specifically, we note that the $LiNi_{0.47}Al_{0.03}Mn_{0.5}O_2$ cathode material shows only an advantage under small current, with its discharge capacity remaining close to that of the pristine material under large current. This can be because the Al-ion is doped into the lithium layer, which can block lithium diffusion, but with this effect not obvious at lower current. However, in the case of higher current, the Al-ion seriously impedes the migration of lithium ions, which leads to a worsening of the cycling performance. Moreover, when the current returns to 0.2 C, the capacity of the pristine material is almost returned back to the original discharge value. In contrast, the doped electrode shows a capacity loss. This is also because of the Al atoms, which hinder the lithiation of the lithium ion. Figure 5d shows the rate performance of the two materials mentioned at high temperature. At a current density of 0.2 C, 0.5 C, 1 C, and 2 C, the doped material delivers capacities of 215.3, 183.7, 144.3, and 66.2 mAh g^{-1}, respectively. While the specific discharge capacities of the pristine electrode are 195.2, 148.4, 101.5, and 99.7 mAh g^{-1}, respectively. The discharge capacity of the cells is higher at high temperature. This is probably due to lithium ions moving higher at high temperatures. Similarly, we found the doped materials to show clear advantages only at low current with also a capacity loss. In summary, a suitable amount of doping can be used to maintain a stable structure and lower Li/Ni cation mixing, but too much doping can have the opposite effect. Cyclic voltammograms of $LiNi_{0.5}Mn_{0.5}O_2$ and $LiNi_{0.47}Al_{0.03}Mn_{0.5}O_2$ in the range of 3.0–4.8 V at a scan rate of 0.1 mV/s are shown in Fig. S2 (a)–(b). From the results, Al-doping can reduce the potential interval and lower the polarization, which are in good agreement with the electrochemical performance.

Figure 6a–d shows the discharge voltage for $LiNi_{0.5-z}Al_zMn_{0.5}O_2$ ($z = 0.00, 0.03, 0.05, 0.08$) at the third, 50th, 100th, and 150th cycle in the voltage range of 3.0~4.8 V at a constant density 0.2 C. As the cycle number increases, the discharge voltage for $LiNi_{0.5}Mn_{0.5}O_2$ decreases abruptly, while that for $LiNi_{0.5-z}Al_zMn_{0.5}O_2$ ($z = 0.03, 0.05, 0.08$) decreases slowly. To be specific, with increased cycling, the discharge voltage for $LiNi_{0.5}Mn_{0.5}O_2$ decreases from 3.8300 to 3.4927 V over 150 cycles, while that for $LiNi_{0.42}Mg_{0.08}Mn_{0.5}O_2$ decreases slightly from 3.8667 to 3.7154 V, which shows that Al-doping can retard the voltage drop during the discharge-charge state. At the same time, the discharge voltage for $LiNi_{0.5-z}Al_zMn_{0.5}O_2$ ($z = 0.00, 0.03, 0.05, 0.08$) decreases slowly with increasing Al content. Alternatively, it can be seen that the capacity curve (shown in Fig. 6e–h) for different cycles for $LiNi_{0.5-z}Al_zMn_{0.5}O_2$ ($z = 0.00, 0.03, 0.05, 0.08$) has a much smaller gap followed by increased z, which indicates that doped materials have lower polarization compared to $LiNi_{0.5}Mn_{0.5}O_2$. Therefore, Al-doping can lower Li/Ni cation mixing to decrease the polarization during the cycle. From

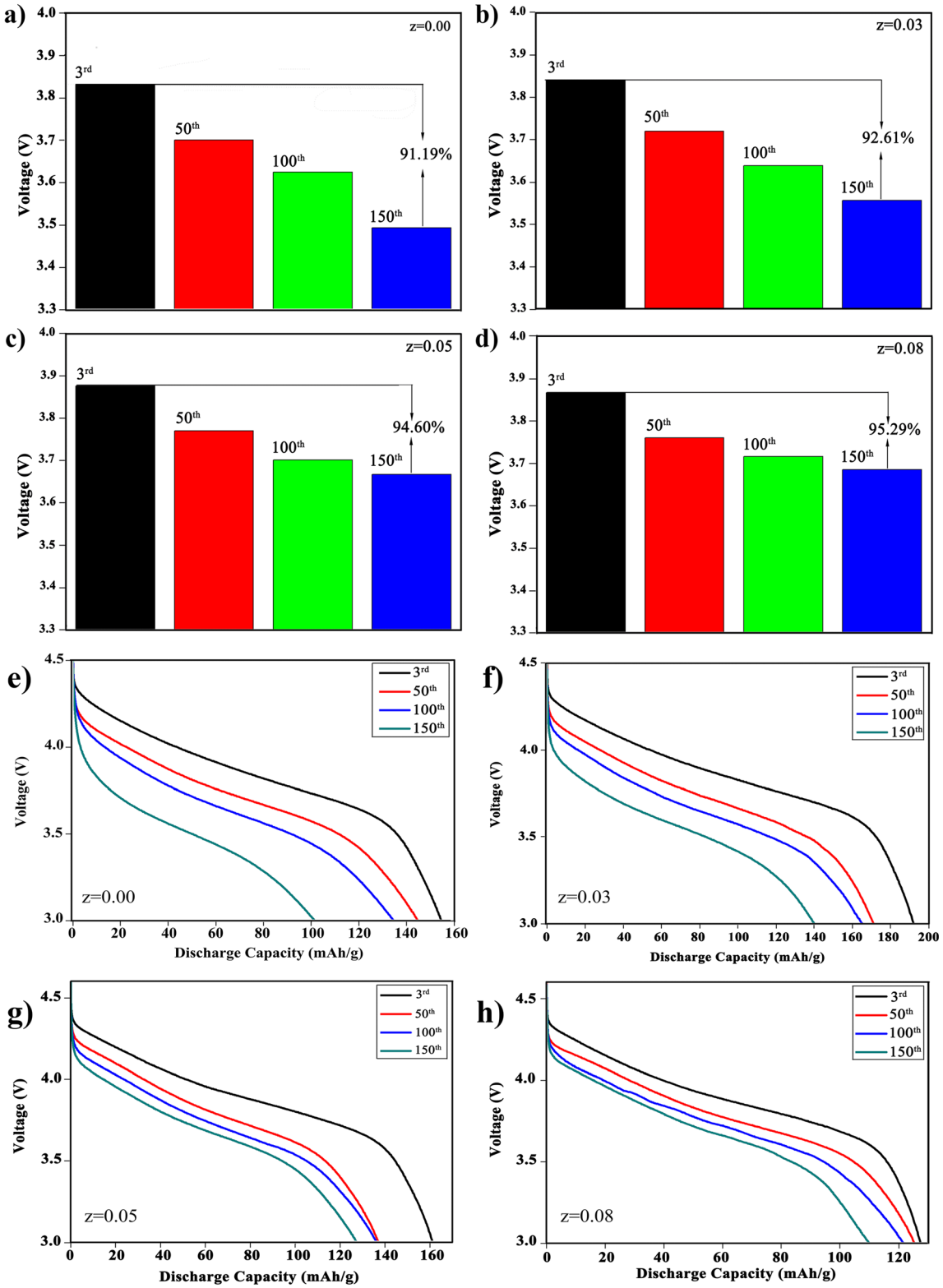

Fig. 6 Discharge voltage after the third, 50th, 100th, and 150th cycles for $LiNi_{0.5-z}Al_zMn_{0.5}O_2$ **a** $z = 0.00$, **b** $z = 0.03$, **c** $z = 0.05$, **d** $z = 0.08$. The discharge capacity at the third, 50th, 100th, and 150th for $LiNi_{0.5-z}Al_zMn_{0.5}O_2$ **e** $z = 0.00$, **f** $z = 0.03$, **g** $z = 0.05$, **h** $z = 0.08$

Fig. 6e–h, the third discharge capacities are 154.7, 192.3, 161.4, and 127.6 mAh g^{-1}, respectively. Compared to these high values, the discharge capacities are 101.5, 140.1, 127.5, and 110.0 mAh g^{-1} at the 150th cycle. With increasing doping, the circulation stability is improved, indicating that doping is beneficial for the structural stability of the materials.

Comprehensive consideration of the result of capacity and voltage decay reveals that the $LiNi_{0.47}Al_{0.03}Mn_{0.5}O_2$ has better electrochemical performance. This result indicates that tiny differences in structure, which can be caused by Al content, can bring about different electrochemical performances.

To characterize changes in the material after circulation, we dissembled the circulating battery, removed the positive plate, cleaned it three times with pure ethyl methyl carbonate (EMC), and carried out XRD tests after drying. The XRD patterns for the post-cycled plate are shown in Fig. 7; the results from the Rietveld refinement are shown in Table 2. The data show that compared with the original material, the crystal cell parameters for the cycled $LiNi_{0.5-z}Al_zMn_{0.5}O_2$ ($z = 0.00, 0.03, 0.05, 0.08$) show small changes. The variation in parameters decreases with increasing z. Therefore, Al-doping can stabilize the material structure even after repeatedly undergoing lithiation/delithiation, with larger doping content leading to a smaller exchange. This conclusion is consistent with the results of the cyclic stability shown in Fig. 6. Previous studies have shown that the (003) slab will expand because of increased repulsion brought on by the more direct meeting between oxygen atoms. As shown in Fig. 7a, we can observe structural changes in $LiNi_{0.5-z}Al_zMn_{0.5}O_2$ ($z = 0.00, 0.03, 0.05, 0.08$)

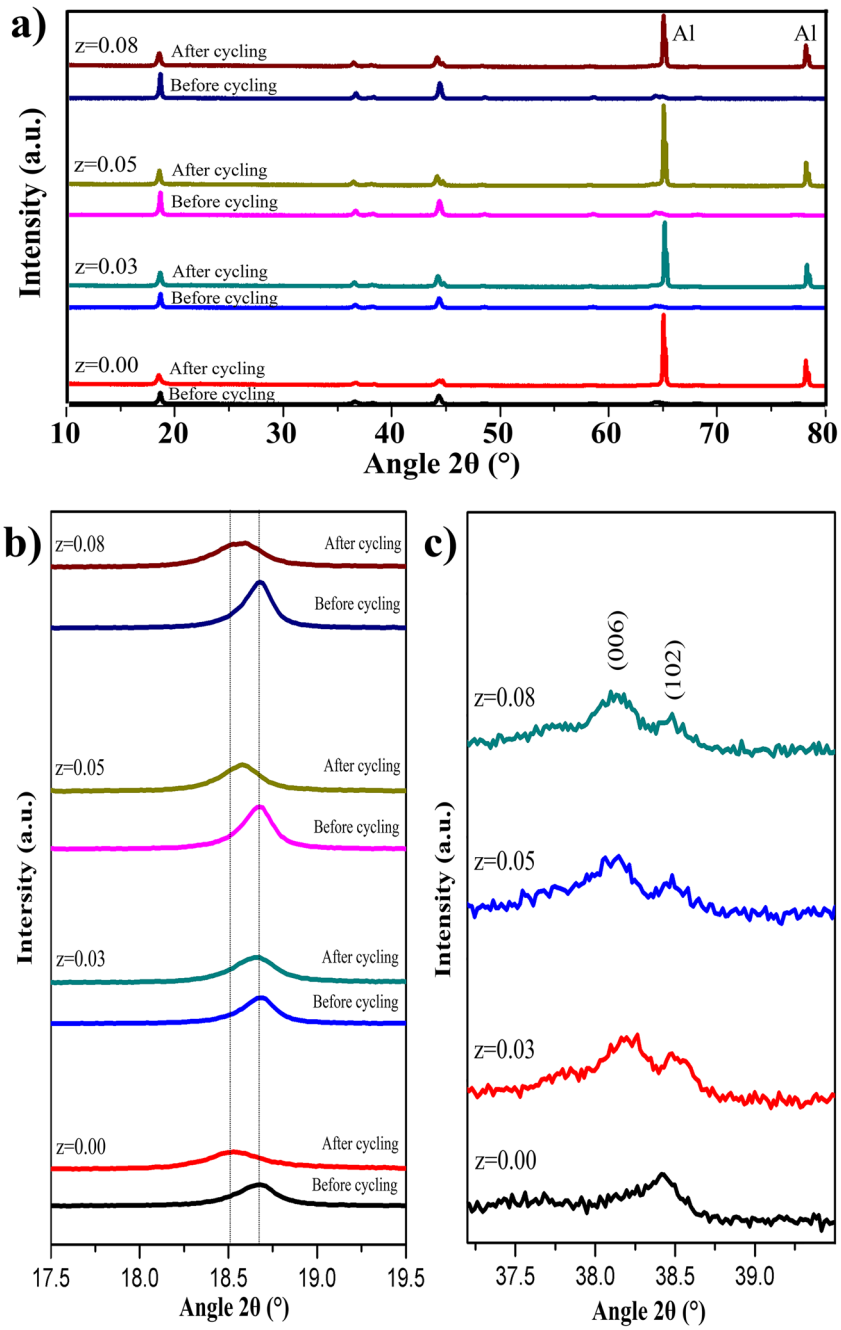

Fig. 7 **a** XRD patterns for the $LiNi_{0.5-z}Al_zMn_{0.5}O_2$ ($z = 0$, 0.03, 0.05, 0.08) electrodes before and after 150 cycles. The exchange of the **b** (003) peak and **c** (006)/(102) peak

Table 2 The crystal cell parameters for $LiNi_{0.5-z}Al_zMn_{0.5}O_2$ ($z = 0$, 0.03, 0.05, 0.08) after cycling

		$z = 0.00$	R	$z = 0.03$	R	$z = 0.05$	R	$z = 0.08$	R
a (Å)	Before	2.8803	0.42%	2.8762	0.30%	2.8737	0.21%	2.8723	0.17%
	After	2.8923		2.8847		2.8797		2.8774	
c (Å)	Before	14.2606	0.50%	14.2542	0.43%	14.2501	0.21%	14.2491	0.19%
	After	14.3370		14.3159		14.2801		14.2775	
V (Å^3)	Before	102.457	1.38%	102.107	1.04%	101.916	0.63%	101.808	0.56%
	After	103.867		103.167		102.556		102.375	

*R is the rate of change

before and after cycling. We find that no impurity peak appears after circulation. Some reports have shown that the (003) slab will expand after cycling because of the increased repulsion caused by the more direct meeting between oxygen atoms [38, 39]. Therefore, the lower the left shift of the (003) peak the higher the reversible capacity. Detailed information for the (003) and (006)/(102) peaks is shown in Fig. 7b and c. Firstly, after 150 cycles, the (003) peak for $LiNi_{0.5}Mn_{0.5}O_2$ shows a clear shift to the left in all materials, which indicates that the reversible capacity of this material is the smallest. This conclusion is consistent with previous electrochemical measurements. In comparison to the un-doped simple, the (003) peak for $LiNi_{0.5-z}Al_zMn_{0.5}O_2$ ($z = 0.03$, 0.05, 0.08) shifts only slightly to the left after 150 cycles, which indicates that the doping makes the structure more stable, in agreement with a much reduced loss of reversible capacity for the doped materials. In particular, the $LiNi_{0.47}Al_{0.03}Mn_{0.5}O_2$ sample shows a minimal left shift, which demonstrates that it has the highest reversible capacity following cycling, in good agreement with the test results for cyclic performance. The (003) peak for the $LiNi_{0.45}Al_{0.05}Mn_{0.5}O_2$ and $LiNi_{0.42}Al_{0.08}Mn_{0.5}O_2$ electrodes shifts to the left slightly more than for $LiNi_{0.47}Al_{0.03}Mn_{0.5}O_2$, which results in a loss of irreversible capacity that is bigger than observed for $LiNi_{0.47}Al_{0.03}Mn_{0.5}O_2$ after 150 cycles. Figure 7c shows the exchange of the splitting peaks of (006)/(102) at approximately 39° after cycling. It should be clear that the (006)/(102) splitting peaks for the pristine sample almost disappear after cycling, while the same peaks in the doped samples still clearly exist following cycling. The splitting of the (006)/(102) peaks can be indexed as a signature for a well-ordered layered structure of the hexagonal type. The disappearance of the two splitting peaks of (006)/(102) for $LiNi_{0.5}Mn_{0.5}O_2$ indicates the destruction of the layered structure after 150 cycles, which can also be further confirmed by the observed broadening for the (003) peak. In contrast, the two splitting peaks of (006)/(102) for $LiNi_{0.5-z}Al_zMn_{0.5}O_2$ ($z = 0.03$, 0.05, 0.08) still clearly exist after 150 cycles, indicating that the layered structure is well maintained due to the doping effect of Al.

Differences in resistance between the un-doped sample and the $LiNi_{0.47}Al_{0.03}Mn_{0.5}O_2$ sample were demonstrated using electrochemical impedance spectroscopy, as shown in Fig. 8a. The inset in Fig. 8a shows the equivalent circuit model used to fit the measured spectra. Rel, Rs, and Rct demote the electrolyte resistance, solid electrolyte interface resistance and charge-transfer resistance, respectively. C and W represent the capacitance and Warburg impedance, respectively. The resistance results are shown in Table 3. As shown in Table 3, the charge transfer resistance for the $LiNi_{0.5}Mn_{0.5}O_2$ and $LiNi_{0.47}Al_{0.03}Mn_{0.5}O_2$ electrodes are 131.1 and 104.1 Ω before cycling, respectively, which indicates that Al-doping can reduce the barrier for lithium-ion transfer.

To explore the impact of the Al-doped material on electrochemical performance, we calculate the Li-ion diffusion coefficient (D_{Li}). D_{Li} is calculated using the following

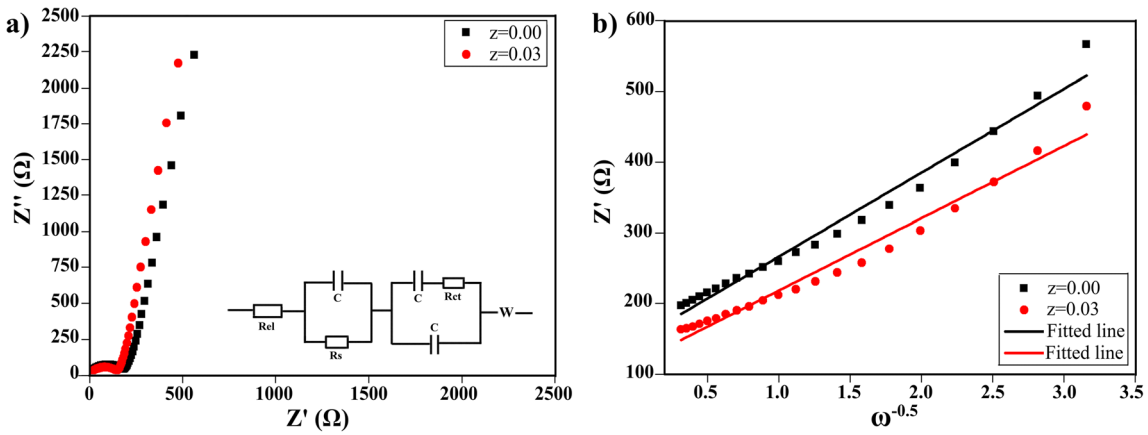

Fig. 8 **a** Nyquist plots for the $LiNi_{0.5}Mn_{0.5}O_2$ and $LiNi_{0.47}Al_{0.03}Mn_{0.5}O_2$ electrodes before cycling. **b** Plot of Z' vs. ω^{-05}

Table 3 Resistances obtained from equivalent circuit fitting of the experimental data for $LiNi_{0.5}Mn_{0.5}O_2$ and $LiNi_{0.47}Al_{0.03}Mn_{0.5}O_2$

Sample	Pristine		
	Rel (Ω)	Rs (Ω)	Rct (Ω)
$LiNi_{0.5}Mn_{0.5}O_2$	1.768	27.25	131.1
$LiNi_{0.47}Al_{0.03}Mn_{0.5}O_2$	3.78	23.56	104.1

equation: $D_{Li} = R^2T^2/2A^2n^4F^4C^2\sigma^2$, in which R is the molar gas constant, T is the thermodynamic temperature, A is the geometric area of the electrode, n is the number of electrons in the reaction, F is the Faraday constant, and C is the concentration of the active materials. σ has a close relationship with the real part of the Nyquist impedance and the frequency used in the electrochemical impedance spectroscopy test. The slope of the $Z\text{-}\omega^{-1/2}$ curve is σ. As shown in Fig. 8b, the un-doped sample has a σ that is approximately 1.2 times greater than that for the $LiNi_{0.47}Al_{0.03}Mn_{0.5}O_2$ sample, which indicates that the D_{Li} value for the $LiNi_{0.47}Al_{0.03}Mn_{0.5}O_2$ sample is 2.4 times larger than that for the un-doped sample. Hence, Al-doping can improve the lithium-ion migration rate. This finding may be attributable to Al-doping lowering the amount Li/Ni cation mixing and reducing the energy barrier for lithium-ion transfer.

Conclusions

$LiNi_{0.5-z}Al_zMn_{0.5}O_2$ ($z = 0$, 0.03, 0.05, 0.08) cathode materials were successfully prepared via a combination of co-precipitation and the solid-state method. The structural changes (before and after cycling) and the electrochemical performance of the cathodes were systematically analyzed. The results of the structural analysis showed that all of the materials before cycling exhibit good crystallinity and a layered structure. However, after cycling, un-doped materials showed a large structural change, leading to the formation of an incomplete layered structure. In addition, $LiNi_{0.47}Al_{0.03}Mn_{0.5}O_2$ can lower Li/Ni cation mixing, increase structural stability, reduce polarization, decrease migration resistance and improve the migration rate of the lithium-ion, which, in turn, enhances the electrochemical properties (including the highest capacity and improved cycle stability) of $LiNi_{0.5}Mn_{0.5}O_2$. The reasons for this enhanced performance are diverse, but the key reason is the doping content. Additionally, the charge transfer resistance of the $LiNi_{0.47}Al_{0.03}Mn_{0.5}O_2$ cathode material is considerably smaller than that of the un-doped material, which indicates a faster lithium-ion migration rate. This finding is in good agreement with the calculated results.

Funding information This work was supported by the Natural Science Foundation of China (U1507106 and U1507114), the Natural Science Foundation of Qinghai Province (2016-GX-101), the Hunan Provincial Science and Technology Plan Project (Nos. 2016TP1007 and 2017TP1001), the Hunan Provincial Science and Technology Plan Project (No. 2016TP1007).

References

1. Thackeray MM, Kang S-H, Johnson CS, Vaughey JT, Benedek R, Hackney SA (2007) Li2MnO3-stabilized LiMO2 (M = Mn, Ni, co) electrodes for lithium-ion batteries. J Mater Chem 17(30):3112–3125
2. Armstrong AR, Holzapfel M, Novak P, Johnson CS, Kang S-H, Thackeray MM, Bruce PG (2006) Demonstrating oxygen loss and associated structural reorganization in the lithium battery cathode LiNi0.2Li0.2Mn0.6O2. J Am Chem Soc 128(26):8694–8698
3. Ohzuku T, Ueda A, Nagayama M, Iwakoshi Y, Komori H (1993) COMPARATIVE-STUDY OF LICOO2, LINI1/2CO1/2O2 AND LINIO2 FOR 4-VOLT SECONDARY LITHIUM CELLS. Electrochim Acta 38(9):1159–1167
4. Kong JZ, Ren C, Jiang YX, Zhou F, Yu C, Tang WP, Li H, Ye SY, Li JX (2016) Li-ion-conductive Li2TiO3-coated li Li0.2Mn0.51Ni0.19Co0.1O2 for high-performance cathode material in lithium-ion battery. J Solid State Electrochem 20(5):1435–1443
5. Kim JK, Manthiram A (1997) A manganese oxyiodide cathode for rechargeable lithium batteries. Nature 390(6657):265–267
6. Armstrong AR, Bruce PG (1996) Synthesis of layered LiMnO2 as an electrode for rechargeable lithium batteries. Nature 381(6582): 499–500
7. Alessandrini F, Conte M, Passerini S, Prosini PP (2001) Overview of ENEA's projects on lithium batteries. J Power Sources 97-8:768–771
8. Brandt K (1995) PRACTICAL BATTERIES BASED ON THE SWING SYSTEM. J Power Sources 54(1):151–154
9. Huang HT, Bruce PG (1994) A 4V lithium manganese oxide cathode for rocking-chair lithium-ion cells. J Electrochem Soc 141(9): L106–L107
10. Shpak AY, Swamy SKK, Dittmer J, Vlasenko NY, Globa NI, Andriiko AA (2016) Formation of stable phases of the li-Mn-co oxide system at 800 a degrees C under ambient oxygen pressure. J Solid State Electrochem 20(1):87–94
11. Ganesh KS, Reddy BP, Kumar PJ, Jayanthbabu K, Rosaiah P, Hussain OM (2015) Microstructural and electrochemical properties of LiTi (y) co (1-y) O-2 film cathodes prepared by RF sputtering. J Solid State Electrochem 19(12):3621–3627
12. Li J, Wan L, Cao C (2016) A high-rate and long cycling life cathode for rechargeable lithium-ion batteries: hollow LiNi0.5Mn0.5O2 nano/micro hierarchical microspheres. Electrochim Acta 191:974–979
13. Liu YM, Cao F, Chen BL, Zhao XZ, Suib SL, Chan HLW, Yuan JK (2012) High performance of LiNi0.5Mn0.5O2 positive electrode boosted by ordered three-dimensional nanostructures. J Power Sources 206:230–235
14. Liu Y, Chen B, Cao F, Zhao X, Yuan J (2011) Synthesis of nanoarchitectured LiNi0.5Mn0.5O2 spheres for high-performance rechargeable lithium-ion batteries via an in situ conversion route. J Mater Chem 21(28):10437
15. Mizuno F, Hayashi A, Tadanaga K (2003) All-solid-state lithium secondary batteries using a layer-structured LiNi0.5Mn0.5O2 cathode material. J Power Sources 124(1):170–173
16. Labrini M, Saadoune I, Scheiba F, Almaggoussi A, Elhaskouri J, Amoros P, Ehrenberg H, Brotz J (2013) Magnetic and structural

approach for understanding the electrochemical behavior of LiNi0.33Co0.33Mn0.33O2 positive electrode material. Electrochim Acta 111:567–574
17. Singh G, Thomas R, Kumar A, Katiyar RS (2012) Electrochemical behavior of Cr- doped composite Li2MnO3-LiMn0.5Ni0.5O2 cathode materials. J Electrochem Soc 159(4):A410
18. Zhao E, Chen M, Chen D, Xiao X, Hu Z (2015) A versatile coating strategy to highly improve the electrochemical properties of layered oxide LiMO(2) (M = Ni0.5Mn0.5 and Ni1/3Mn1/3Co1/3). ACS Appl Mater Interfaces 7(49):27096–27105
19. Peng C, Jin J, Chen GZ (2007) A comparative study on electrochemical co-deposition and capacitance of composite films of conducting polymers and carbon nanotubes. Electrochim Acta 53(2):525–537
20. Svegl F, Orel B, Grabec-Svegl I, Kaucic V (2000) Characterization of spinel Co3O4 and li-doped Co3O4 thin film electrocatalysts prepared by the sol-gel route. Electrochim Acta 45(25–26):4359–4371
21. Zhang X, Jiang WJ, Mauger A, Qilu GF, Julien CM (2010) Minimization of the cation mixing in Li1-x(NMC)(1-x)O-2 as cathode material. J Power Sources 195(5):1292–1301
22. Reale P, Privitera D, Panero S, Scrosati B (2007) An investigation on the effect of li+/Ni2+ cation mixing on electrochemical performances and analysis of the electron conductivity properties of LiCo0.33Mn0.33M0.33O2. Solid State Ionics 178(23–24):1390–1397
23. Okamoto K, Shizuka K, Akai T, Tamaki Y, Okahara K, Nomura M (2006) X-ray absorption fine structure study on layered LiMO2 (M = Ni, Mn, co) cathode materials. J Electrochem Soc 153(6):A1120–A1127
24. Zhao EY, Chen MM, Hu ZB, Xiao XL, Chen DF (2016) Layered/layered Homostyructure ion conductor coating strategy for high performance Lithium ion batteries. Electrochim Acta 208:64–70
25. Dou SM, Wang WL, Li HJ, Xin XD (2011) Synthesis and electrochemical performance of LiNi0.475Mn0.475Al0.05O2 as cathode material for lithium-ion battery from Ni-Mn-Al-O precursor. J Solid State Electrochem 15(4):747–751
26. Yang G, Zhao E, Chen M, Cheng Y, Xue L, Hu Z, Xiao X, Li F (2017) Mg doping improving the cycle stability of LiNi0.5Mn0.5O2 at high voltage. J Solid State Electrochem
27. Kang SH, Kim J, Stoll ME, Abraham D, Sun YK, Amine K (2002) Layered li(Ni0.5-xMn0.5-xM '(2x))O-2 (M ' = co, Al, Ti; x = 0, 0.025) cathode materials for li-ion rechargeable batteries. J Power Sources 112(1):41–48
28. Pan CJ, Lee YJ, Ammundsen B, Grey CP (2002) Li-6 MAS NMR studies of the local structure and electrochemical properties of Cr-doped lithium manganese and lithium cobalt oxide cathode materials for lithium-ion batteries. Chem Mater 14(5):2289–2299
29. Myung ST, Komaba S, Hosoya K, Hirosaki N, Miura Y, Kumagai N (2005) Synthesis of LiNi0.5Mn0.5-xTixO2 by an emulsion drying method and effect of Ti on structure and electrochemical properties. Chem Mater 17(9):2427–2435
30. Chen M, Zhao E, Chen D, Wu M, Han S, Huang Q, Yang L, Xiao X, Hu Z (2017) Decreasing li/Ni disorder and improving the electrochemical performances of Ni-rich LiNi0.8Co0.1Mn0.1O2 by ca doping. Inorg Chem 56(14):8355–8362
31. Wang D, Li X, Wang Z, Guo H, Xu Y, Fan Y, Ru J (2016) Role of zirconium dopant on the structure and high voltage electrochemical performances of LiNi0.5Co0.2Mn0.3O2 cathode materials for lithium ion batteries. Electrochim Acta 188:48–56
32. Hu G, Zhang M, Liang L, Peng Z, Du K, Cao Y (2016) Mg–Al–B co-substitution LiNi0.5Co0.2Mn0.3O2 cathode materials with improved cycling performance for lithium-ion battery under high cut-off voltage. Electrochim Acta 190:264–275
33. Han CJ, Eom WS, Lee SM, Cho WI, Jang H (2005) Study of the electrochemical properties of Ga-doped LiNi0.8Co0.2O2 synthesized by a sol–gel method. J Power Sources 144(1):214–219
34. Li F, Yang G, Jia G, Shangguan X, Zhuge Q, Bai B (2017) Improvement in the electrochemical performance of a LiNi0.5Mn0.5O2 cathode material at high voltage. J Appl Electrochem
35. Kaneda H (2017) Improving the Cycling Performance and Thermal Stability of LiNi0.6Co0.2Mn0.2O2 Cathode Materials by Nb-doping and Surface Modification. International J Electrochem Sci :4640–4653
36. Wang Y, Yang Z, Qian Y, Gu L, Zhou H (2015) New insights into improving rate performance of Lithium-rich cathode material. Adv Mater 27(26):3915–3920
37. Chen J, Tan X, Liu H, Guo L, Zhang J, Jiang Y, Zhang J, Wang H, Feng X, Chu W (2017) Understanding the underlying mechanism of the enhanced performance of Si doped LiNi0.5Mn0.5-xSixO2 cathode material. Electrochim Acta 228:167–174
38. Zhang J, Gao R, Sun L, Zhang H, Hu Z, Liu X (2016) Unraveling the multiple effects of Li2ZrO3 coating on the structural and electrochemical performances of LiCoO2 as high-voltage cathode materials. Electrochim Acta 209:102–110
39. Yang G, Jia G, Shangguan X, Zhu Z, Peng Z, Zhuge Q, Li F, Bai B (2017) The synergistic effects of Li2SiO3-coating and Si4+−doping for LiNi0.5Mn0.5O2 cathode materials on the structure and the electrochemical properties. J Electrochem Soc 164(12):A2889–A2897